Earth Sciences
2021; 10(2): 36-48
http://www.sciencepublishinggroup.com/j/earth
doi: 10.11648/j.earth.20211002.11
ISSN: 2328-5974 (Print); ISSN: 2328-5982 (Online)

Mapping the Alteration Zones for Uranium Exploration in Gabal Abu Garadi Area Central Eastern Desert, Egypt, Using Aster Data

Nehal Mohamed Soliman[1], Moustafa Bayoumi Bayoumi[2, *], Salem Mohamed Salem[1]

[1]National Authority for Remote Sensing and Space Sciences (NARSS), Cairo, Egypt

[2]Nuclear Materials Authority (NMA), Cairo, Egypt

Email address:

moustafanma@yahoo.com (M. B. Bayoumi)

[*]Corresponding author

To cite this article:

Nehal Mohamed Soliman, Moustafa Bayoumi Bayoumi, Salem Mohamed Salem. Mapping the Alteration Zones for Uranium Exploration in Gabal Abu Garadi Area Central Eastern Desert, Egypt, Using Aster Data. *Earth Sciences*. Vol. 10, No. 2, 2021, pp. 36-48.
doi: 10.11648/j.earth.20211002.11

Received: February 16, 2021; **Accepted**: March 15, 2021; **Published**: April 23, 2021

Abstract: The integration of the ASTER image processing and the airborne spectrometric Gamma-Ray interpretation helped in identifying the types and illustrating the distributions of the probable sites for radioactive mineralization at the Gabal Abu Garadi area. Appling various techniques of image processing for Landsat OLI and ASTER satellite to discrimination the differently exposed rock units and extract major and minor structural lineaments. This study resulted that the ASTER VNIR-SWIR bands are effectively used for clarifying the sericite, kaolinite, chlorite, illite and hematite bearing alteration zones, whereas the ASTER TIR bands are most effective in delineation of the silica-rich zones which could be pathfinders for radioactive mineralization within the study area. The resultant alteration maps show good coincidence with the explored uranium sites and suggest further similar unexplored sites. The predominance of low eTh/eU= 1.31 indicates U mobilization and reveals that magmatic differentiation was not the sole process responsible for the concentration of these radioactive elements in the Abu Gradi area. Where the presence of adequate structures such as shear zones and fault planes facilitates the circulation of hydrothermal fluids and meteoric waters leading to mobilization and a redistribution of uranium. This paper could assist the principals of uranium exploration techniques.

Keywords: Abu Garadi, Remote Sensing, Radioactive Mineralization, GIS Data, Eastern Desert

1. Introduction

Granitiod rocks cover meny localities at Eastern Desert of Egypt. Gabal Abu Garadi granitic rocks are important plutons in the studied district as they could be promising sites for radioactive minerals. The boarders of study area lies between latitudes 25° 33 - 25° 40 N and longitudes 34° 2 - 34° 14 E, (Figure 1). They are widely distributed as separate and continued hills of moderate to high peaks, showing intrusive contacts with the surrounding country rock of the volcanic and gabbroid rocks. Hussein et al., and Cambon, [1, 2] considered the younger granitic rocks are to be good targets for uranium prospection. The Nuclear Materials Authority of Egypt (NMA) surveyed most of the granitic plutons for the purpose of identification and registration of the most important radioactive localities in Egypt. Remote sensing techniques provides detailed geological information and important for mineral mapping and lithological discrimination. By which several authors discussed the usage of ASTER data as a powerful tool for lithologic (lithological) mapping and delineation of hydrothermal alteration, (Rowan et al.; Goetz et al.; Boardman et al.; Kruse et al.; Zoheir and Lehmann; Pour and Hashim. El-Said, M, et Al., [2, 3, 4, 5, 6, 7] and [8], applied the Processing of Multispectral ASTER Data for Mapping Alteration Minerals Zones: As an Aid for Uranium Exploration in Elmissikat-Eleridiya Granites, Central Eastern Desert, Egypt. Salem and Soliman [9] used ASTER data in the identification of alteration z ones in the metavolcanics for gold prospecting at the eastern end of Wadi Allaqi, S. Eastern Desert, Egypt and Salem et, al. [10]

used of Aster data and geochemical analysis for the exploration of gold at Samut (Samut) area, South Eastern Desert, Egypt. Salem "et al.". 2018 [11] used of Aster data and geochemical analysis for the exploration of gold at Samut (Samut) area, South Eastern Desert, Egypt. The concept of the band rationing technique was widely used in different areas (Rowan et al., Hewson et al., Massironi et al., Hadi and Najeeb, Zoheir and Emam, Pour and Hashim, Hassan et al., Mohy et al., Kurata and Yamaguchi, Wang et al., [12-20]. Ratio images are. More information can be obtained by using those ratios that maximize the differences in the spectral slopes of materials in the scene. The main idea of this study aims to exploring of the uranium occurrences in the grantiod rocks which are suitable pathfinders for carrying different radioactive minerals especially through the alteration zones in such rocks. So the differentiating of the alteration zones from their host granitic rocks by the ASTER imagery is the rule and the govern of this work.

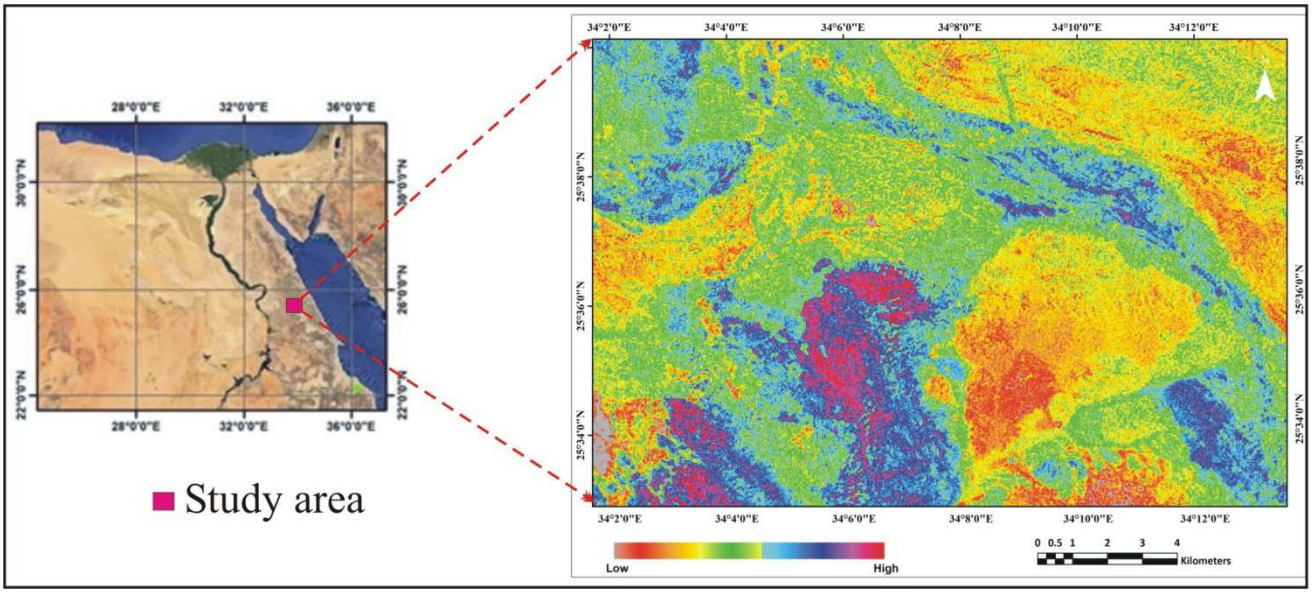

Figure 1. *Location of Gabal Abu Garadi, Central Eastern Desert, Egypt.*

2. Geological Setting

The studied area consists mainly of serpentine and related rocks, metasediments, sediments, older granites (gray granites), Hammamat sediments, younger granites and Phanerozoic volcanic, (Figure 2). The focusing study mainly on the geology of Gabal Abu Garadi and Gabal Atawi younger granites as they are the valid and target rocks for radioelement's exploration. Gabal Abu Garadi is a remarkable landmark of monzogranites having an oval shape oblated in the ENE direction with 1*2 Km length. Gabal Atawi granitic rocks consists of two main granitic stocks of different forms, sizes and extensions. The large stock is an oval shape, trends ENE direction with 5*9 km length. It exhibits a fine grained chilled margin against its country rocks. These granites are pale pink in color, massive, un-deformed, extensively jointed. They range in size from fine, medium to course grained show porphyritic texture in parts, and highly weathered and fractured. The coarse granite is pink color, megacrystic and encountered in the southwestern part of the platoon. The medium grained granites variety is a pale pink color and form most of the northern and eastern parts of the pluton. Locally, it is highly fractured and tectonized. The fine grained granite is whitish pink color and exposed at the extreme northeastern part of the Pluton and altered to albitized granites. They intruded the surrounding older metamorphosed schistose metavolcanics with sharp intrusive contacts. These rocks are traversed by post-granitic dykes and veins. Dykes represented by acidic and basic dykes, while veins represented by mineralized quartz vein and fluorite vein. Structurally, the study area is influenced by several minor and major faults characterized by alteration features such as silicification, hematization, albitization and kaolinization.

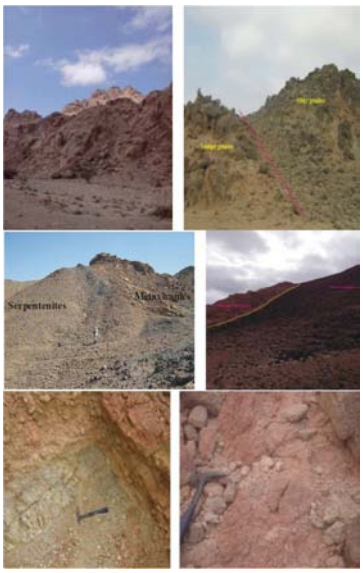

Figure 2. *Field photographs, shows the different rock unites and its relations at Gabal Abu Garadi.*

3. Methodology

For finalizing and conclude the results of this study, using the ASTER data and geological field observations supported by air born spectrometric analysis. The ASTER L1B product is a registered radiance at sensor data. Therefore, several pre-processing techniques were applied to subset data covering the study area to be suitable for further image processing techniques.

3.1. Image Processing Data

ASTER data (free level IB ASTER VNIR & SWIR data Granule ID: ASTL1B 0403150819140808041013) - acquired on March 15, 2008 - were digitally pre-processed for geo-referencing, atmospheric, and radiometric cross-talk correction of ASTER-SWIR bands, layer stacking of VNIR-SWIR bands in unique nine bands data-cube, and ortho-rectification of data using SRTM topographic data. These are performed by ENVI 4.7 and ArcGIS ver. 10.5 through the conversion of the data to real-world coordinates on the area maps to improve the quality of the raw data. Analysis of images was carried out using ENVI 5.3 and ArcGIS version 10.1 software. For geological and structural features as well as for lithological discrimination, false color composite (FCC) and band rations (BR) have been performed. The lineaments which reflect the passages of the mineral bearing hydrothermal solution were extracted automatically from the principal component image (PC1) as favorable areas valid for mineral explorations. For alteration zone mapping, Constrained Energy Minimization (CEM) and Crosta PC techniques have been used as follows;

3.2. Airborne Data

The available airborne radio spectrometric data scale 1:50,000 were surveyed by Aero-Service Division, Western Geophysical Company of America, USA, in 1984 (Aero-Service [21]. The survey was conducted at a flight altitude of 120 m terrain clearance, 1.5 km of flight line interval, and 10 km of tie line spacing. These data have been prepared for subsequent processing by digitizing the maps in numeric format that permits the application of interpolation (gridding) technique. Radio spectrometric data have been subjected to separation of the obtained radio spectrometric measurements over every rock unit, remobilization index map: The construction of the (eU-eTh/3.5) map enables to delineate the limits between the negative contours (leaching) and positive contours (deposition), Clarke et al., [22].

4. Results

4.1. False Color Composite FCC

FCC of ASTER bands (7, 5 and 2 in RBG) has illustrated the main geological and structural features, and discriminated the different rock units, differentiated between the plutonic and volcanic rocks in which the plutonics appear in pale greenish blue color and the volcanics in a pale pinkish gray color and. (Figure 3).

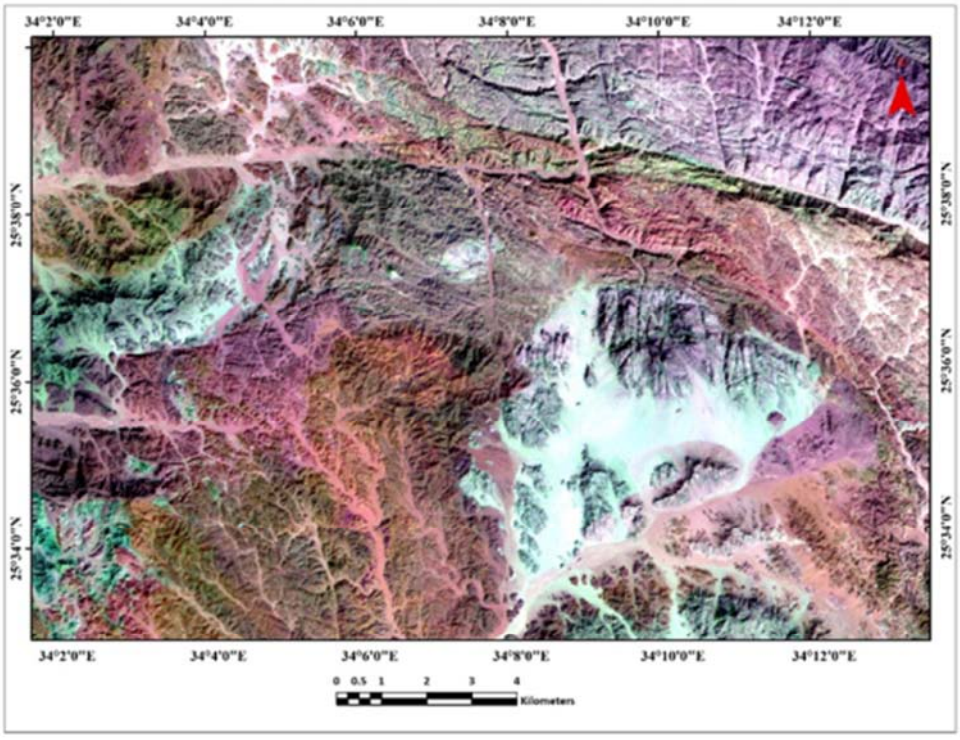

Figure 3. *ASTER false color composite (FCC) (7-5-2) image of Gabal Abu Garadi area.*

4.2. Band Ratio Combinations

ASTER band ratio 8/5, 5/4, 7/8 has differentiated three phases of younger granites in the study area. The oldest phase is biotite granite, followed by gray biotite muscovite

pink granite, and then the youngest phase is of muscovite granite in the Gabal Abu Garadi area (Figure 4). Moreover, ASTER ratio image (4/5, 4/6 and 4/7) highlighted the hydrothermal alterations as bright colors (Figure 5).

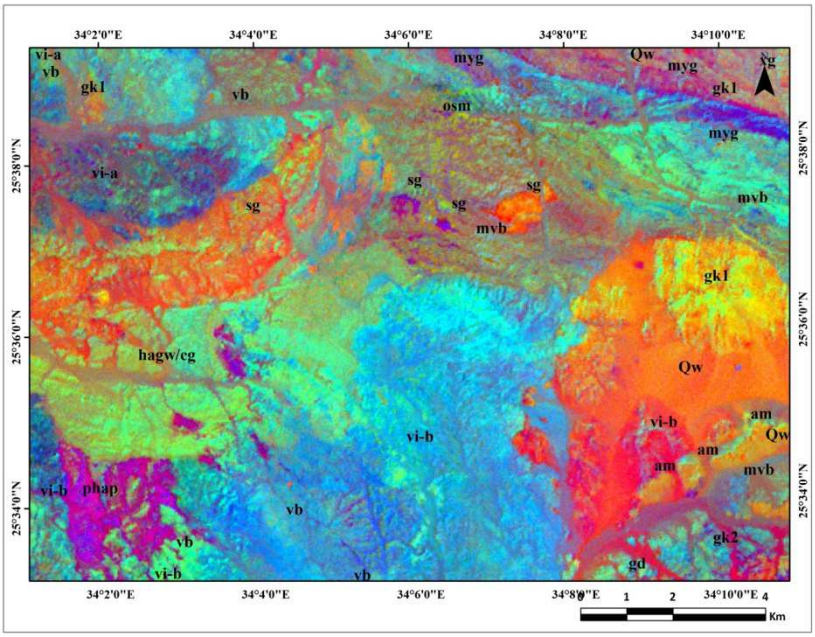

Figure 4. *ASTER band ratio image 8/5, 5/4, 7/8 in RGB. Showing different phases of granites in Gabal Abu Garadi.*

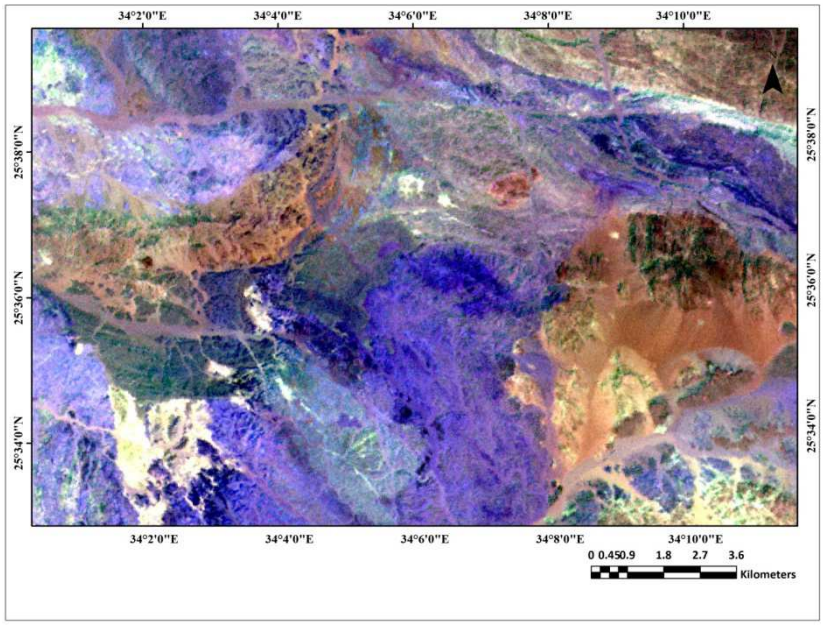

Figure 5. *Band ratio image 4/5, 4/6, 4/7 in RGB. Showing hydrothermal alterations as bright colors, at Gabal Abu Garadi.*

4.3. Crosta Principal Component (Crosta PC)

The result of Crosta PC approach revealed presence of hydrothermal minerals (Table 1).

Chlorite

Eigenvectors for the VNIR-SWIR domains show that PC4 has high positive loading from band 1 (0.815920) and negative from band 8 (-0.456703). Result shows chloritization as green colored areas (Figure 6A).

Epidote

PC2 band 6 (-0.611119) has the highest negative signed loading and positive signed loading from band 8 (0.217363). The resultant image represents epidote mineral as cyan (Figure 6B).

Hematite

PC2 band 9 (0.626927) has high positive loading and band 4 (-0.740060) is negative. Resultant image represents hematite mineral as red color (Figure 6C).

Illite

PC4 band 7 (-0.780831) has highest negative signed loadings and positive sign at band 8 (0.602099). The illite mineral image represents as orange color (Figure 6D).

Kaolinite

PC2 band 6 (-0.811566) has the highest negative signed

loadings and band 7 (0.569685) a positive sign. The image of kaolinite mineral is represented by blue color (Figure 6E).

Montmorillonite

PC4 band 7 (-0.608695) has a high negative loading and positive sign band9 (0.765045). The montmorillonite mineral occurs as a purple color (Figure 6F).

Alunite

PC3 band 5 (-0.608695) has a high negative loading and band 9 (0.765045) is positive sign. The montmorillonite mineral occurs as a yellow color (Figure 6G).

Sericite

PC4 band 7 (-0.780831) has the highest negative sign and band 8 (0.602099) has positive sign. The sericite alteration occurs by magenta color (Figure 6H).

Table 1. *ASTER bands for Chlorite, Kaolinite, Illite, Alunite, Epidote, Sericite, Montmorillonite, and Hematite.*

CHLORITE

Eigenvector	Band 1↑	Band 2	Band 5↑	Band 8
PC1	0.515795	0.507374	0.489372	0.486869
PC2	0.170291	-0.174048	0.684547	-0.687098
PC3	-0.198066	-0.709719	0.409085	0.538256
PC4	0.815920	-0.456703	-0.352930	-0.033714

EPIDOTE

Eigenvector	Band 3	Band 5↑	Band 6↑	Band 8
PC1	0.678490	0.369034	0.411093	0.484218
PC2	0.518300	-0.557362	-0.611119	0.217363
PC3	-0.514368	-0.187158	0.031902	0.836289
PC4	0.080262	-0.719815	0.675662	-0.137501

HEMATITE

Eigenvector	Band 2↑	Band 3	Band 4↑	Band 9
PC1	0.551084	0.597278	0.506244	0.288587
PC2	-0.125292	0.208750	-0.740060	0.626927
PC3	-0.123295	-0.571990	0.410326	0.699470
PC4	0.815725	-0.522024	-0.166316	-0.185532

ILLITE

Eigenvector	Band 4	Band 6	Band 7	Band 8
PC1	-0.571345	-0.413033	-0.517647	-0.484778
PC2	-0.767730	0.005383	0.327077	0.550983
PC3	-0.272173	0.900928	-0.123956	-0.314460
PC4	0.100388	0.133052	-0.780831	0.602099

KAOLINITE

Eigenvector	Band 4↑	Band 6	Band 7↑	Band 9
PC1	0.609853	0.442826	0.539602	0.375253
PC2	0.782033	-0.301311	-0.339702	-0.426893
PC3	0.005503	-0.811566	0.569685	0.129574
PC4	0.128348	-0.233404	-0.518547	0.812501

MONTOMORONITE

Eigenvector	Band 3↑	Band 6	Band 7↑	Band 9
PC1	0.671245	0.404871	0.511097	0.352547
PC2	0.684386	-0.602259	-0.160887	- 0.378174
PC3	-0.241771	-0.672132	0.585137	0.383927
PC4	0.150310	-0.146979	-0.608695	0.765045

ALUNITE

Eigenvector	Band 3↑	Band 5	Band 7↑	Band 9
PC1	-0.683911	-0.36883	-0.51887	-0.356383
PC2	-0.688522	0.540043	0.231794	0.424926
PC3	-0.180882	-0.749817	0.508823	0.382303
PC4	-0.159638	0.100478	0.646642	-0.739103

SERICITE

Eigenvector	Band 4↑	Band 6	Band 7↑	Band 8
PC1	-0.571345	-0.413033	-0.517647	-0.484778
PC2	-0.767730	0.005383	0.327077	0.550983
PC3	-0.272173	0.900928	-0.123956	-0.314460
PC4	0.100388	0.133052	-0.780831	0.602099

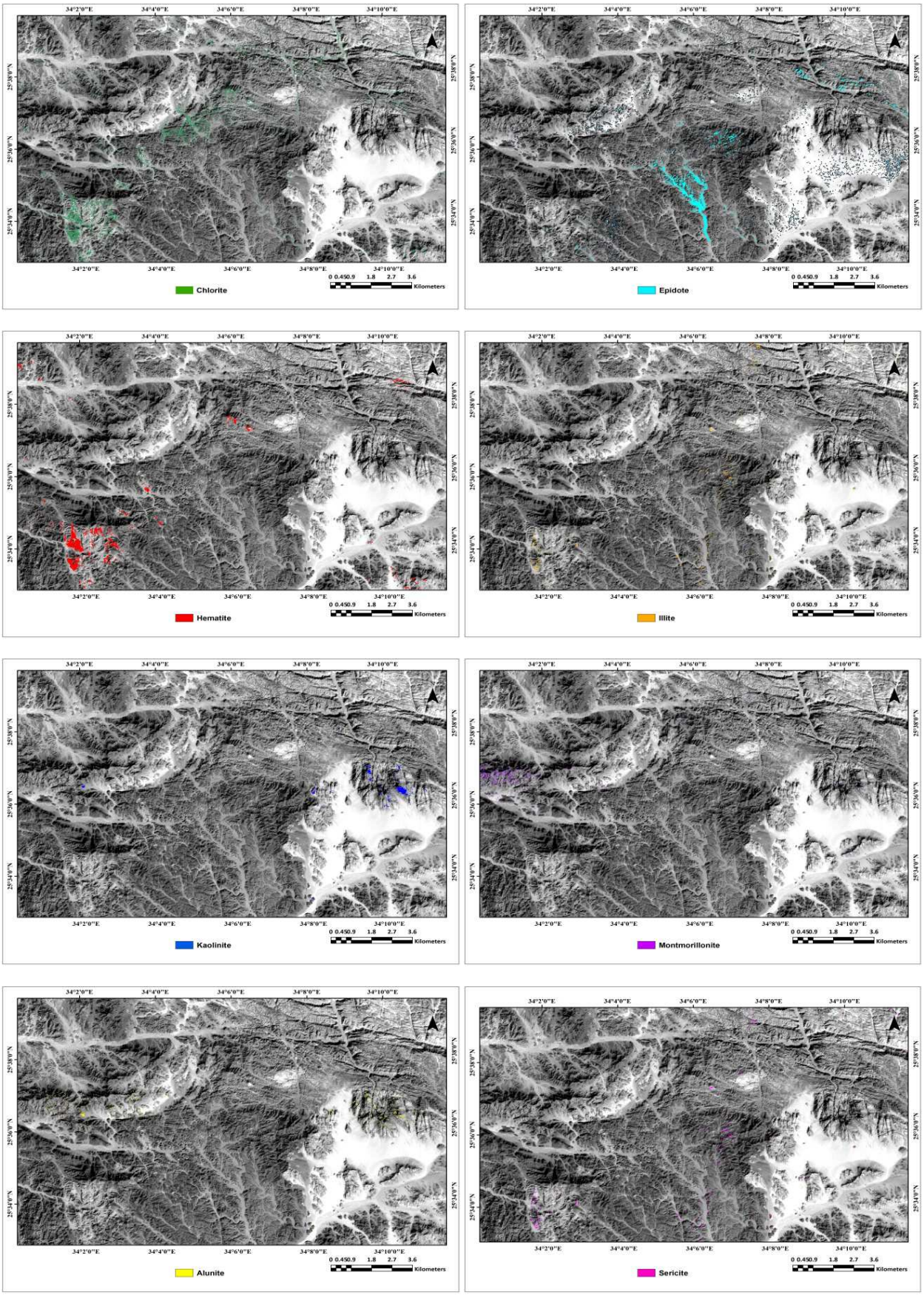

Figure 6. *(A) PC4 Chlorite image. (B) PC2 Epidote image. (C) PC2 Hematite image (D) PC4 Illite image (E) PC2 Kaolinite image. (F) PC4 Montmorillonite image (G) PC3 Alunite image. (H) PC4 Sericite image. At Gabal Abu Garadi area, Central Eastern Desert, Egypt.*

5. Constrained Energy Minimization (CEM) Technique

Constrained Energy Minimization (CEM) appear as a series of gray scale images, one for each selected endmember. Stretching setting provides good visibility for small features. If needed, you can apply a different stretch so that larger features in the image are visible. The curves of the selected minerals are selected from USGS library (Figure 7). Thres holding were applied to show the higher concentration area by using the equation (Elsaied et al., 2014). Showing the alteration minerals (Figure 8a-f).

Band DN Threshold = Mean + 2*(Standard deviation)

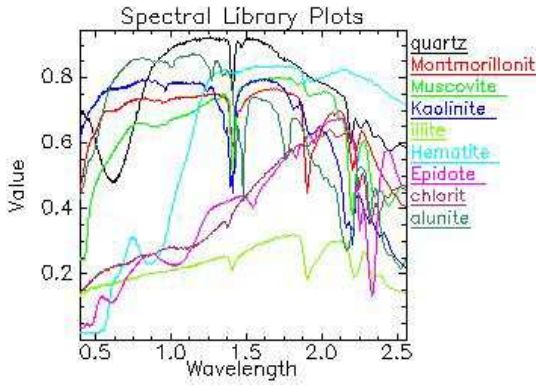

Figure 7. *The USGS library spectra of the studied minerals superimposed on ASTER data band intervals in the VNIR-SWIR region.*

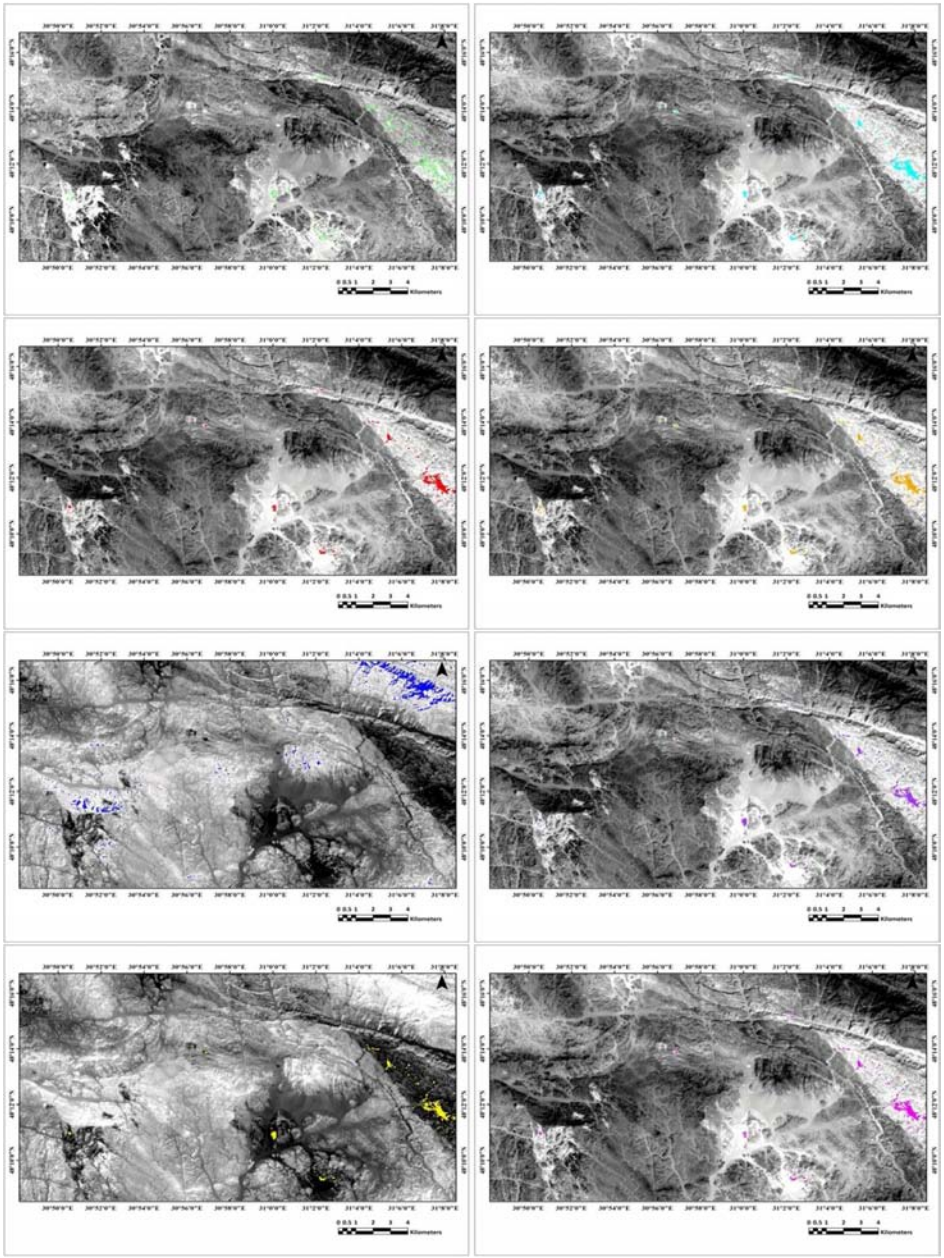

Figure 8. *Separated CEM classification endmember (chlorite, epidote, hematite, illite, kaolinite, montmorillonite, alunite and sericite) using VNIR-SWIR stack and the USGS ASTER resampled a spectral library, at Gabal Abu Garadi.*

6. Lineament Extractions

The coincidence of high-density lineaments and alteration zones indicate a high probability for the presence of mineralization. Thus, the lineament density map became more useful when it is combined with other information regarding the alteration zones; thus we used the result of the CEM technique as that represents the spatial distribution of the alteration minerals. Accordingly, we can identify the most potential areas of mineralization taking us into consideration the overlapping of high lineament density areas with abundant alterations (Figure 9).

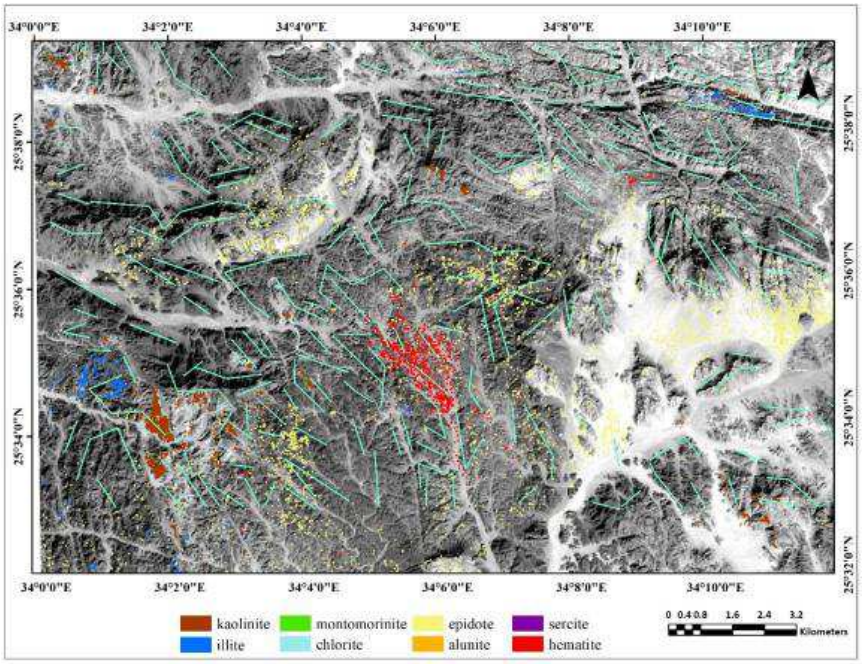

Figure 9. *CEM classified endmembers and lineaments overlying grey scale image, at Gabal Abu Garadi area.*

7. Interpreted Geologic Map

For constructing a geologic map using remote sensing techniques, band combination (7, 5, 2, in RBG), band ratio combination (8/5, 5/4, 7/8, in RGB), Principle Component Analysis (PCA) integrated with field observations, whereas band ratio combination was used to distinguish between phases of granites G. Abu Garadi. Comparing the resultant geological map with the previously published map of Abdel-Kader et al., [23], reveals the accuracy of the obtained map and the fine discrimination of the rock units. Integration between the results, derived from the processed ASTER images and previous works demonstrates the efficiency of these techniques in lithological mapping of Gabal Abu Garadi area (Figure 10).

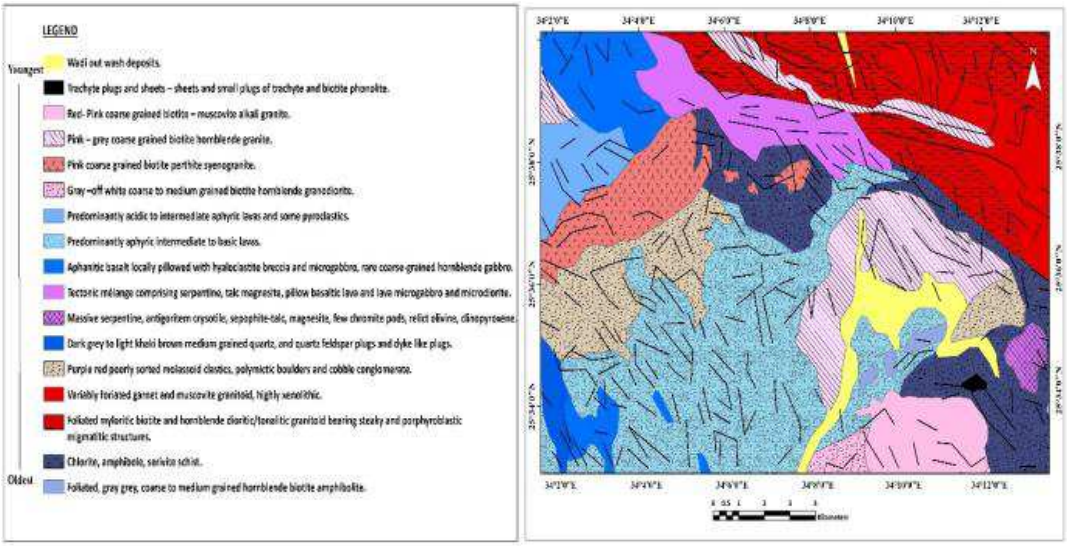

Figure 10. *Geologic map of Gabal Abu Garadi.*

8. Gamma-ray Spectrometric Survey in the Study Area

8.1. Total Count Contour Map

Correlation between the radiometric contour map (Figure 11) with respective geologic units and Image processing shows that the radioactivity of the study area ranges form 20-120 Ur (younger granite). Radiometric map show also the sharp remarkable delineation at the contacts between the younger granite phases, radioactivity ranges between (10 to 30Ur). Granite of main plutons ranges in radioactivity from 40 to 60 Ur, which cleared by green countour lines and 30 to 70Ur colored by red colors at other places of the plutons but violet contour lines ranges from 70-120Ur were conceder anomaly zones. It is encountered as large radioactive anomaly elongated in the NE-SW direction.

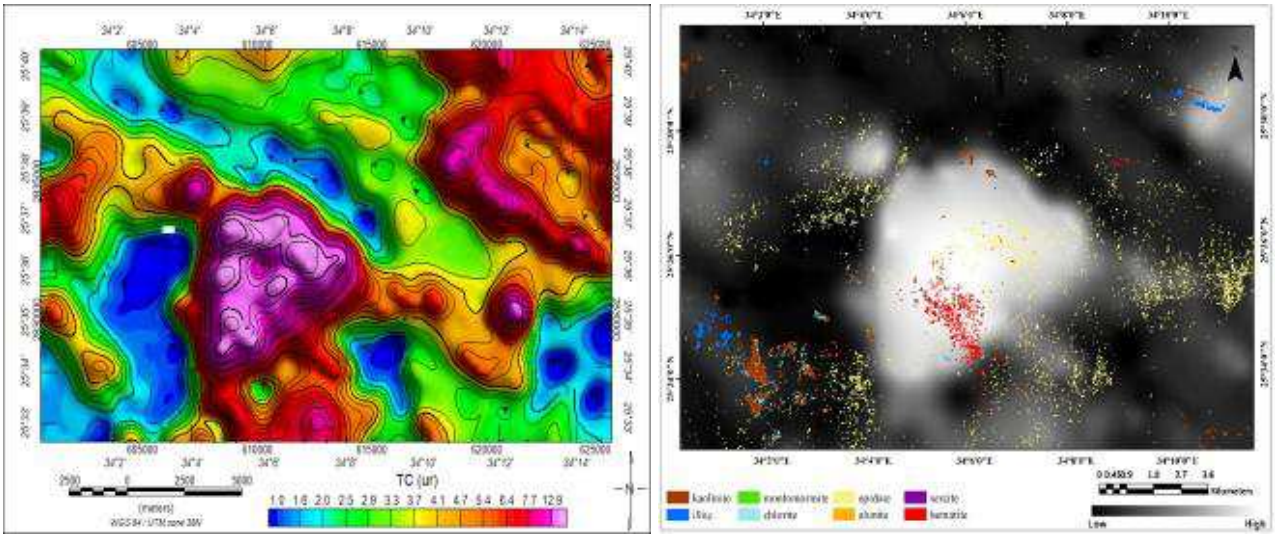

Figure 11. *Total count contourmap with alterations map, in Ur (×10), abal Abu Garadi.*

8.2. Potassium Contour Map

The potassium surface distribution (Figure 12) shows younger granite has high level K-content, ranging in intensity from 0.3 to 5.5%. It is defined as concentric contours bounded the plutons with contour line 2.8% which separated it from the lowest radioactive levels of granites and wadi sediments. The younger granitic plutons has number of elongated anomalies >5% mostly concentrated in the center of the younger granitic bodies. These anomalies are separated from each other and affected mainly by the NW-SE and NE-SW faults. The lowest potassium values (<1.6%) are associated mainly with the sheared basic dike, which is well discriminated from the country rocks, with its elongated shape and low K level, trending in the NW-SE direction. The wadis around the granites show potassium concentrations values ranging from 0.2 to 1.6%.

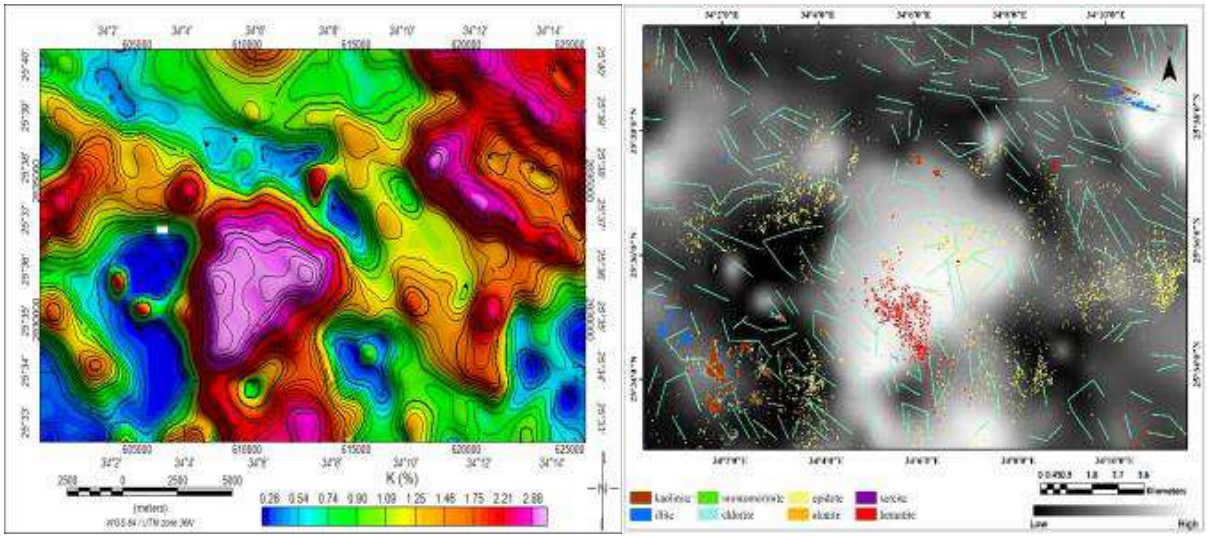

Figure 12. *Potassium percentage contour map with alterations and lineaments map, in Ur (×10), Gabal Abu Garadi.*

8.3. Uranium Contour Map

Generally, the shape and trends of the contour lines agree with the trend of the total count map (Figure 11). The correlation between uranium distribution contour map (Figure 13) and the geological map indicates that the sites of uranium can accumulated in it, firstly younger granites and acidic rocks, secondly fault systems which dissected the main plutons. Uranium content varies between (20 to 120 ppmeU) over younger granites. Contour lines of >130 ppmeU represent uranium anomalies which generally elongated in the NE-SW direction with oval shape. Two small anomalies, with values reaching 120 ppmeU, are located to the southwest of the studied area that are associated with the alteration zones and faults. The EW-SE faults separate other anomalies with moderate values and limited extension. Whereas, the sheared basic dyke characterized by narrow elongated high eU anomaly that trending in the EW direction reaches its maximum values of about 30 ppmeU which illustrated by green contour lines. The wadi sediments are not showing discriminated trends for uranium content and their level are less than 10ppm which illustrated by blue contour lines.

8.4. Thorium Contour Map

Thorium is an immobile element and each rock unit has its own Th signature during the magmatic differentiation, the distribution of thorium can be used as a geological indicator. So, Th-content coincide with one lithologic unit differ from the other rock types as shown in (Figure 14). The range of eTh in younger granite plutons ranges from 25 ppm to 160 ppm and this rock type considered as eTh anomaly in the study area, whereas wadi sediments ranges from 1.1 to 10 ppm eTh. The highly differentiated granite of the area under investigations is delineated with the eTh contour line of 10 ppm with increasing the values toward the center of the plutons. The center of the plutons has major anomaly elongated along the NW-SE direction. This anomaly separated into three zones, due to the dominant EW-SW faults, with different values increasing toward the northwest reaching its maximum values of 160 ppm.

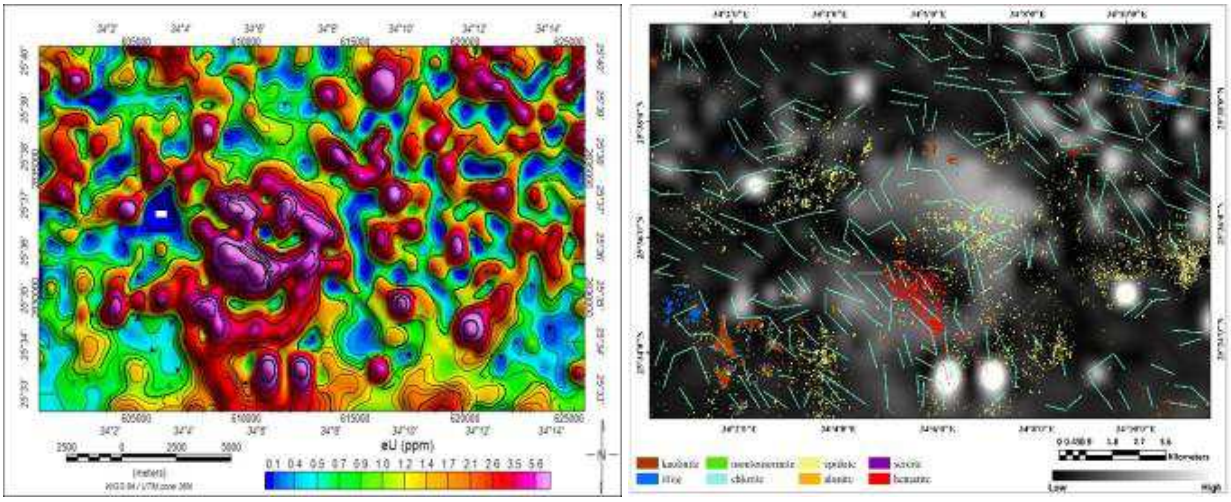

Figure 13. *Equivalent uranium contour with alterations and lineaments map, Gabal Abu Garadi.*

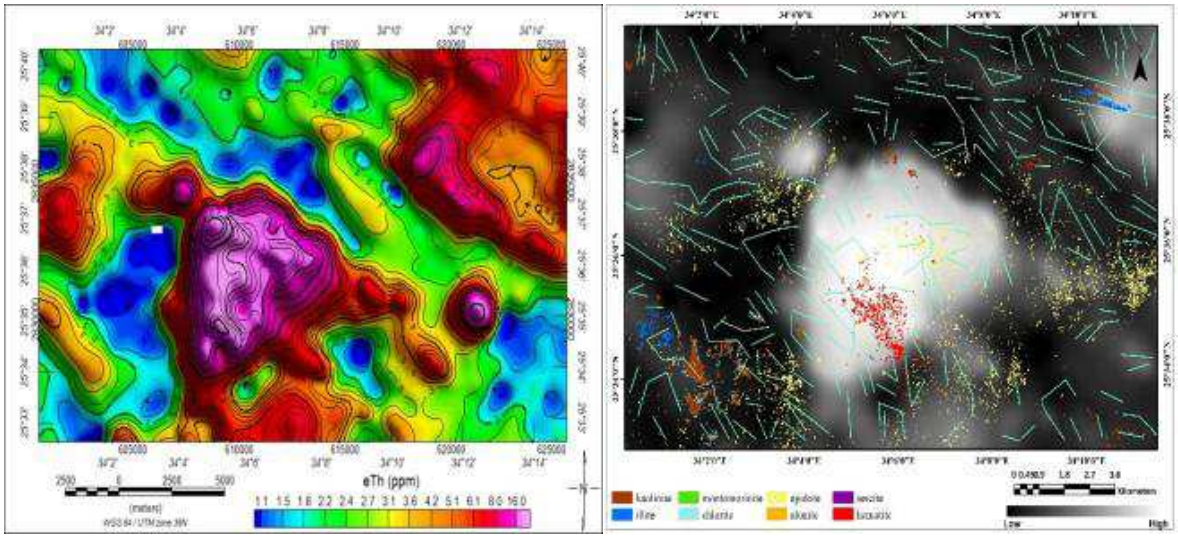

Figure 14. *Equivalent thorium contour with alterations and lineaments map, Gabal Abu Garadi.*

8.5. Uranium Migration Index Contour Map

Conversion of uranium from the four (4) oxidizing state to six oxidizing state give ability to react with another elements and migrate from its source to another position so to get an idea about the remobilization of uranium in the area, the expected original contents of uranium is calculated by dividing eTh content by the Clark eTh/eU ratio (3-4) in granite (Clark et. al. 1966). The result is the hypothetical uranium distribution. It is very helpful to define the trends of uranium migration. The eU-(eTh/3.5) remobilization parameter contour map (Figure 15) shows good coincidence with the high eU concentrations. There are very high anomalies up to >240 that appear as closed and dense violet color, mainly over the sheared basic dike that trending in the EW direction. Other high anomalies of about 50-95 are associated with the younger granite. The red and violet lines represent the possible sites and directions of uranium mobilization. The process of uranium mobilization towards the sheared basic dike is very important; as such an altered rock is subjected to mineralization-bearing solutions. The direction of uranium migration may be from the different rock bodies to the fault planes and sheared rocks.

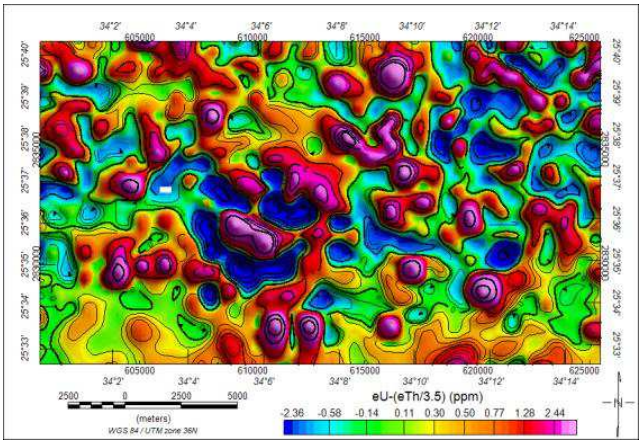

Figure 15. *eU-(eTh/3.5) contour map, Gabal Abu Garadi.*

9. Results and Discussion

These techniques were used successfully in lithological discrimination of uranium-bearing granites, in addition to characterization and mapping the hydrothermal alteration zones that usually help in localization of uranium mineralization. Spectrometry data in VNIR, SWIR and TIR spectral regions through different image classification methods reveal the following spectral characteristics for younger granites: ASTER RGB bands 7, 5, 2 color composite image showed good contrast between the granitic rocks and their country rocks within the studied areas, ASTER band ratio 8/5, 5/4, 7/8 showed the best false-color composite image with Optimum Index Factor (OIF = 68.03) in mapping the different rock units of the study area, where it could discriminate the granitic rocks from the country rocks and succeed in delineate the contact between different types of granites, metasedements and volcanics in Gabal Abu Garadi area. Using the Band Ratio 4/5, 4/6, 4/7 gives good results in mapping the alteration end members of younger granites, especially in ASTER VNIR and SWIR bands, where most distinctive absorption features of clay minerals are present. Using ASTER ratio indices in VINR, SWIR and TIR spectral regions, such as ferric iron index, ferrous iron index, Gossan index (Iron oxides index), Hydroxyl-bearing mineral Index, phyllic index, argillic index, alunite index, kaolinite index and quartz index revealed locations of alteration zones with high concentrations of clay, that are highly correlated with radioactive anomalies and alteration zones, as follows: Iron indices maps; there are differences in concentrations of both ferrous and ferric iron distribution in the study area, where, ferric index. Further detailed airborne gamma-ray spectrometric measurements along with this study should be integrated with higher spectral resolution imagery (like hyperspectral data); in order to delineate alteration zones and new mineralization sites more precisely.

10. Conclusions and Recommendations

1. For achieve the main goal of this study, applying these techniques where is successfully in uranium explorations and delineated the localization of uranium mineralization sites and uranium-bearing granites, the lithological discrimination of different rock types in addition to characterization and mapping the hydrothermal alteration zones.
2. The ASTER image spectrometry data in VNIR, SWIR and TIR spectral regions through different image classification methods reveal the following spectral characteristics for younger granites: ASTER RGB bands 7, 5, 2 color composite image showed good contrast between the granitic rocks and their country rocks within the studied areas, ASTER band ratio 8/5, 5/4, 7/8 showed the best false-color composite image with Optimum Index Factor (OIF = 68.03) in mapping the different rock units of the study area, where it could discriminate the granitic rocks from the country rocks and succeed in delineate the contact between different types of granites, metasedements and volcanics in Gabal Abu Garadi area.
3. Using the Band Ratio 4/5, 4/6, 4/7 gives good results in mapping the alteration end members of younger granites, especially in ASTER VNIR and SWIR bands, where most distinctive absorption features of clay minerals are present.
4. Using ASTER ratio indices in VINR, SWIR and TIR spectral regions, such as ferric iron index, ferrous iron index, Gossan index (Iron oxides index), Hydroxyl-bearing mineral Index, phyllic index, argillic index, alunite index, kaolinite index and quartz index revealed locations of alteration zones with high concentrations of

clay, that are highly correlated with radioactive anomalies and alteration zones.

5. Further detailed airborne gamma-ray spectrometric measurements along with this study should be integrated with higher spectral resolution imagery (like hyperspectral data); in order to delineate alteration zones and new mineralization sites more precisely.
6. The results from the present study were evaluated using a visual overlay analysis to quantify the accuracy of mapping that could not be carried out due to restrictions in the length of the this work. It is, therefore, suggested that future studies should mathematically evaluate the accuracies achieved in such a study using, predictive models such as the weights of evidence method.

This study avoids many disadvantages that may arise due to human activities, spectral variations, shades and topography. Structural lineaments play an important rule governing alteration zones along with radionuclide distribution, as they represent the pathways of the carrier solutions (hydrothermal or meteoric types). The results from the present study were evaluated using a visual overlay analysis; a statistical evaluation to quantify the accuracy of mapping, therefore, suggested that future studies should mathematically evaluate the accuracies achieved in such a study using, predictive models such as the weights of evidence method.

Acknowledgements

The authors thanks Remote Sensing and GIS Department, Nuclear Materials Authority for facilitating image processing methods.

References

[1] Cambon, A. R. (1994) Uranium deposites in granitic rocks. Notes on the National tranining course on uranium geology and exploration. Organized by IAEA and NMA, 8-20 Jan.

[2] Rowan, L. C., Goetz, A. F. H., Ashley, R. P. (1977) Discrimination of hydrothermally altered and unaltered rocks in visible and near infrared multispectral images. Geophysics 42 (3): 522–535.

[3] Goetz AFH, Rock B. N., Rowan, L. C. (1983) Remote sensing for exploration, an overview. Econ Geo 78: 573–590 Full Text via bCross Ref View Record in Scopus Cited By in Scopus (43).

[4] Boardman, J. W., Kruse, F. A., Green, R. O. (1995) Mapping target signatures via partial unmixing of AVIRIS data In: Green RO (Ed) Summaries of the Fifth JPL Airborne Earth Science Workshop JPL Publ 95 (1): 23–26.

[5] Kruse, F. A., Boardman, J. W., Huntington, J. F. (2003) Evaluation and Validation of EO-1 Hyperion for mineral mapping. IEEE Trans Geosci Rem Sens 41 (6): 1388–1400. https://doi.org/10.1109/TGRS.2003.812908.

[6] Zoheir, B., Lehmann, B. (2011) Listwaenite-lode association at the Barramiya gold mine, Eastern Desert, Egypt. Ore Geol Rev 39: 101–115 USGS spectral library of rock forming minerals, http:// www.speclab.cr.usgs.gov.

[7] Pour, A. B., Hashim, M. (2012) The application of ASTER remote sensing data to porphyry copper and epithermal gold deposits. Ore Geol Rev 44: 1–9 Cited 37 times.

[8] El Said, M., Abo Elkhair, H., Dardier, A., Hermas, S and Urai Minoru. (2014) Processing of Multispectral ASTER Data for Mapping Alteration Minerals Zones: As an Aid for Uranium Exploration in Elmissikat-Eleridiya Granites, Central Eastern Desert, Egypt. The open Geology Journal, 2014, 8, (sup 11: M5) 69-83.

[9] Salem, M. Salem. and Soliman, N. M. (2015) Exploration of gold at the east end ofWadi Allaqi, South Eastern Desert, Egypt, using remote sensing techniques, Arab J Geosci, (2015), V 8 Issue 11.

[10] Salem, S. M., Soliman, N. M., Ramadan, T. M., Greiling, R. O. (2013) Exploration of new gold occurrences in the alteration zones at the Barramiya District, Central Eastern Desert of Egypt using ASTER data and geological studies. Arab J Geosci 7 (2014): 1717–1731.

[11] Salem, M. Salem., El Sharkawi, M. A. Z., El Alfy and Ahmed, S. E. (2018) The use of Aster data and geochemical analysis for the exploration of gold at samut area, South Eastern Desert, Egypt. Arabian journal of Geoscience (2018) 11; 541.

[12] Rowan, L. C., Hook, S. J., Abrams, M. J. and Mars, J. C. (2003) "Mapping hydrothermally altered rocks at Cuprite, Nevada, using the Advanced Spaceborne Thermal Emission and Reflection Radiometer (ASTER), a new satellite-imaging system." Economic Geology 98 (5): 1019-1027.

[13] Hewson, R. T., Cudahy, S., Mizuhiko, K., Ueda and Mauger A. (2005) "Seamless geological map generation using ASTER in the Broken Hill-Curnamona province of Australia." Remote Sensing of Environment 99 (1-2): 159-172.

[14] Massironi, M. L., Bertoldi, P., Calafa, D. Visonà, A. Bistacchi, C., Giardino and Schiavo, A. (2008) "Interpretation and processing of ASTER data for geological mapping and granitoids detection in the Saghro massif (eastern Anti-Atlas, Morocco)." Geosphere 4 (4): 736-759.

[15] Hadi, G. S. and Najeeb, A. A. Z. (2011) "Using the band ratio classification method to detect the regions that need to remove sedimentation in Tigris River." Iraqi Journal of Science 52 (3): 376-380.

[16] Zoheir, B. and Emam, A. (2012) "Integrated analysis of field, mineralogical and satellite imagery data for geologic mapping and exploration targets in the greenstone terrane of South Eastern Desert, Egypt." J Afr Earth Sci: 66-67.

[17] Hassan, S. M., Sadek, M. F. and Greiling, R. O. (2015) "Spectral analyses of basement rocks in El-Sibai-Umm Shaddad area, Central Eastern Desert, Egypt, using ASTER thermal infrared data." Arabian Journal of Geosciences 8 (9): 6853-6865.

[18] Mohy, H., El-Magd, I. A. and Basta, F. F. (2016) "Newly improved band ratio of ASTER data for lithological mapping of the Fawakhir Area, Central Eastern Desert, Egypt." Journal of the Indian Society of Remote Sensing 44 (5): 735-746.

[19] Kurata, K. and Yamaguchi, Y. (2019) "Integration and Visualization of Mineralogical and Topographical Information Derived from ASTER and DEM Data." Remote Sensing 11 (2): 162.

[20] Wang, Q., Y. Li and H. Hu (2019) "Numerical simulation of remote infrared imaging for marine exhaust system using wide-band k-distribution model combined with a new grouping method for spectral sub-intervals." Infrared Physics & Technology 96: 276-290.

[21] Aero-Service, (1984) Interpretation report of airborne gamma-ray spec- trometer and magnetometer survey of the Eastern Desert of Egypt. Aero-Service Division, Western Geophysical Company of America, USA, pp 1–127

[22] Clarke, S. P. Jr., Peterman, Z. E. and Heier, K. S. (1966) Abundances in uranium, thorium and potassium. In: Handbook of physical constants, Geological Society of America, Memoir 97, p. 521-541.

[23] Abd El kader, Z. M., Ammar, S. E., Abd El wahed, A, A and Sadek, A, A. (2002) D istribution of U and Th in some Granitic masses from the Central Eastern Desert of Egypt. Egyptian Journal of Geology Vol. 46/1 2002: 146-165.